RSC Advances

PAPER

View Article Online
View Journal | View Issue

Cite this: *RSC Adv.*, 2026, **16**, 16854

Unveiling the degradation of lamotrigine in sulfate radical-mediated oxidation: kinetics, influencing factors and transformation mechanisms

Jiayue Dong,[a] Jing Wu,[a] Jialing Zhang,[a] Zhuoming Deng,[a] Guoqiang Liu *[ab] and Yonghua Liu*[a]

Lamotrigine (LMG), a widely used anticonvulsant drug, has been frequently detected in aquatic environments due to its limited removal in conventional wastewater treatment. Here, we systematically investigated the degradation of LMG *via* heat-activated peroxydisulfate (heat/PDS) treatment. The degradation followed pseudo-first-order kinetics, with the observed rate constant (k_{obs}) increasing at higher PDS doses or elevated temperatures. The apparent activation energy was determined to be 88.7 kJ mol^{-1}. Radical quenching experiments using methanol or *tert*-butanol indicated that $SO_4^{\bullet-}$ predominated in LMG degradation. The presence of halides (Br^- and Cl^-), natural organic matter (NOM), ammonium (NH_4^+), or bicarbonate (HCO_3^-) generally inhibited LMG degradation, primarily due to their competition for $SO_4^{\bullet-}$. Detailed transformation pathways were proposed based on quantum chemical calculations and high-resolution mass spectrometry, revealing initial attacks on electron-rich sites of the triazine ring and amino groups, leading to hydroxylated and deaminated products. Both ECOSAR predictions and luminescence bacteria assays showed reduced toxicity for most transformation products relative to LMG, suggesting that degradation of LMG by sulfate radical was a detoxification process. This study demonstrates that heat-activated PDS is an effective strategy for eliminating LMG and attenuating its ecological risk in water.

Received 9th December 2025
Accepted 8th March 2026

DOI: 10.1039/d5ra09514j

rsc.li/rsc-advances

1 Introduction

Lamotrigine (LMG), 6-(2,3-dichlorophenyl)-1,2,4-triazine-3,5-diamine, is a widely prescribed anticonvulsant drug used to treat epilepsy and bipolar disorders.[1] In humans, approximately 70% of the administered dose of LMG is recovered from urine with 90% as the metabolite lamotrigine-N2-glucuronide.[2,3] After excretion, these metabolites can enter the environment and regenerate the parent LMG in favorable conditions. Over the past decade, LMG has been detected in several water environments. The molecular structure of LMG comprises a triazine ring moiety with two amine groups and a benzene ring moiety substituted with two chlorines, contributing to its low volatility and limited lipophilicity, which promote its persistence in aqueous environments.

Ferrer *et al.* first reported the frequent occurrence of LMG in groundwater and surface water, with its concentration ranging from 17 to 488 ng L^{-1}.[4] In wastewater, its concentration can be up to 0.013–1.254 μg L^{-1}.[5–8] Moreover, LMG has been shown to accumulate in soils irrigated with treated wastewater, with concentrations up to 4 mg kg^{-1}, raising concerns about potentially leaching into groundwater.[9] Although studies on the ecotoxicity of LMG remain limited, emerging evidence suggests it may induce oxidative stress and neurotoxicity in aquatic organisms such as fish and has been associated with potential drug–drug interactions in humans.[8,10,11] A recent study demonstrated LMG might translocate in plants, reaching leaves, and affect the expression of stress genes.[12] Yang *et al.* found that the occurrence of LMG in surface water may pose a high risk to the environment ($LD_{50,oral}$ = 205 mg kg^{-1}), potentially inducing oxidative stress and neurotoxicity in fish.[13] Therefore, effective removal of LMG from water environments is imperative to mitigate ecological and public health risks.

Conventional wastewater treatment approaches (WWTPs) showed limited efficacy in LMG degradation.[14,15] For instance, Bollmann *et al.* investigated the transformation and removal of LMG in municipal WWTPs.[14] They found that LMG concentration increased from 1.1 μg L^{-1} in the influent to 1.6 μg L^{-1} in the effluent, implying the poor elimination of LMG. When LMG was subjected to simulated sunlight at pH 7.0, the degradation half-life of over 100 h, implying its high resistance to direct photodegradation as well.[16–18] Karpov *et al.* (2021) demonstrated that redox-active minerals like bimessite (δ-MnO_2) could degrade LMG *via* oxidation, dechlorination, and addition reactions.[19]

[a]*Nanjing Institute of Environmental Science, Ministry of Ecology and Environment of China, Nanjing 210042, China. E-mail: gqliushane@foxmail.com; liuyh@nies.org; Tel: +86-025-85287130*

[b]*State Key Laboratory of Pollution Control and Resource Reuse, School of the Environment, Nanjing University, Nanjing, Jiangsu Province 210023, PR China*

More importantly, phenolic compounds, like vanillic acid, can enhance LMG degradation while leading to the formation of numerous coupling products. These products are more stable than the parent LMG and its long-term ecological impacts remain largely unknown. These findings underscore the need for advanced treatment technologies.

Sulfate radical ($SO_4^{\bullet-}$)-based advanced oxidation processes (SR-AOPs) have emerged as a promising alternative for degrading persistent organic contaminants.[20–23] $SO_4^{\bullet-}$, along with other reactive oxidants (*i.e.* $^{\bullet}OH$ or $O_2^{\bullet-}$), can be generated from the activation of peroxymonosulfate (PMS) or peroxydisulfate (PDS). Several methods have been applied for the activation of persulfates, including the use of UV light, heat, ultrasound, transition metal and others.[24–26] Among these, thermal activation is particularly attractive for its high efficiency, scalability, and practicality for real-world applications. To date, heat activated persulfates have been successfully implemented in wastewater treatment systems, such as hospital effluent. $SO_4^{\bullet-}$ possesses a high oxidation capacity (2.5–3.1 V *vs.* NHE) and a long lifetime ($t_{1/2}$ = 30–40 μs), enabling effective degradation of recalcitrant compounds.[27–29] SR-AOPs has been successfully applied in the degradation of triazine compounds, including atrazine, simazine and propazine.[30–33] Ji *et al.* reported that $SO_4^{\bullet-}$ tends to attack alkylamino side chains of triazine ring in atrazine molecule, leading to hydroxylated products which subsequently undergo decomposition to form ketone or aldehyde.[31] Given the structural similarity of LMG, which also contains a triazine core, it is plausible that $SO_4^{\bullet-}$ could effectively degrade LMG, yet the underlying mechanisms and transformation pathways remain largely unexplored.

Inspired by all above, we attempt to elucidate the degradation of LMG in a heat/PDS oxidation system. Firstly, the effects of operating condition and water matrix (including halides, natural organic matter (NOM), nitrogenous ions, and bicarbonate ion (HCO_3^-)) on kinetics and efficiency of LMG degradation were explored. Then, solid phase extraction-liquid chromatography-mass spectroscopy (SPE-LC-MS), as a powerful tool, was applied to identify transformation products and speculate detailed degradation mechanism and pathway. Finally, the ecotoxicological impacts of LMG and its transformation products in heat/PDS system were assessed using ECOSAR and luminescent bacteria assays. Above all, this study aims to provide theoretical underpinning and technical guidance for remediation of the LMG-contaminated water using $SO_4^{\bullet-}$-based AOPs.

2 Experimental section

2.1 Materials and reagents

All chemicals and reagents used in this work were of the purest quality available. Lamotrigine (LMG), sodium peroxydisulfate ($Na_2S_2O_8$), sodium chloride (NaCl), sodium bromide (NaBr), sodium carbonate (Na_2CO_3), sodium bicarbonate ($NaHCO_3$), sodium nitrate ($NaNO_3$), ammonium sulfate ($(NH_4)_2SO_4$), potassium dihydrogen phosphate (KH_2PO_3) and sodium hydroxide (NaOH) were purchased from Aladdin (Shanghai, China). Suwannee River NOM was supplied by the International Humic Substances Society (St. Paul, MN, USA). Methanol (MEOH) and *tert*-butyl alcohol (TBA) were of high-performance liquid chromatography (HPLC) degrade and purchased from Thermo Fisher (MA, USA). Ultra-pure water (18.2 MΩ cm^{-1}) was used in all prepared solution.

2.2 Experiments setup

The degradation of LMG in heat/PDS was performed in the thermostatic water bath for 180 min. Appropriate volume of LMG stock solution was transferred into a series of cylindrical glass vials and specific aliquots of PDS stock solution were added to achieve a total 50 mL reaction solution with pre-determined concentration. The PDS concentration varied from 0 to 2 mM and the temperature was set from 40 °C to 80 °C. The pH was maintained at 7.0 using 10 mM phosphate buffer. Parallel experiments with additional 10 mM MEOH or TBA were conducted identically to investigate the role the oxidant radicals. Effects of halides (Cl^- and Br^-), SRNOM, nitrogenous ions (NH_4^+ and NO_3), and HCO_3^- were also investigated. At preset intervals, reaction aliquots (1 mL) were collected and immediately transferred to the vial in ice bath to stop the reaction, then stored at 4 °C before HPLC analysis.

To identify the transformation products of LMG, 200 mL reaction solution containing 10 μM LMG, 1 mM PDS, 10 mM phosphate buffer was allowed to reaction for 180 min in a 60 °C water bath. At pre-determined intervals, the samples were withdrawn and immediately transferred to ice bath to quench the reaction. After that all the solutions were enriched into 1 mL MEOH with C18 solid phase extraction (SPE) and stored in a 4 °C refrigerator before HRMS analysis. Detailed procedure of SPE was displayed in Text S1. All samples were stored in a 4 °C refrigerator at most 24 h before analysis.

2.3 Analytical methods

Concentration of LMG was determined by a Shimadzu 20AD HPLC (Shimadzu, Japan) equipped with a photo-diode array detector (SPD-M20A). Separation was performed on Agilent Zorbax Eclipse Plus C18 reverse phase column (4.6 × 250 mm, 5 μm). The injection volume was 30 μL, and the flow rate was 1.0 mL min^{-1}. The mobile phase was composed of 70% MEOH and 30% water. The retention time and detection wavelength of LMG were 5.42 min and 316 nm, respectively.

LMG and its degradation products were identified by a high-resolution mass spectrometer (HRMS) comprised of a HPLC equipped with a Q-Exactive mass spectrometer (Thermo Fisher Scientific, USA). Elution was performed at a flow rate of 0.2 mL min^{-1} with water and MeOH, employing a linear gradient as follows: 95% A, 0–3 min; 95% to 5% A, 3–7 min; 5% A, 7–12 min; 5% to 95% A, 12–12.1 min; 95% A, 12.1–15 min. The sample injection volume was 2 μL. Mass analyses were conducted in negative mode using electrospray ionization (ESI) source. The instrument parameters used for sample analysis were as follows: ion transfer tube temperature of 350 °C; source temperature of 300 °C; sheath gas pressure of 35 arb, auxiliary gas pressure of 10 arb, spray voltage of 3500 V. Mass spectrometric data was collected at full scan mode over a mass range of *m*/*z* 60–900 to identify the degradation products.

2.4 Density functional theory calculations

Density functional theory (DFT) calculations were performed *via* Gaussian 16 quantum chemistry computation package. The optimization of the molecular geometry of LMG was performed at M062x/6-31g+(d) level of theory. Solvation model based on density (SMD) was used to investigate the solvent effect of water. All the computed frequencies of the optimized structure were positive, which means the energy stability of the structure. The highest occupied molecular orbital (HOMO) of LMG was obtained from Gaussview 6 software dependent on the checkpoint file from Gaussian 16. Moreover, the electrophilic Fukui function was calculated to predict reactive sites of electrophilic attack.[34,35] This function was defined as follows:

$$f(r) = \left(\frac{\partial^2 E}{\partial N \times \partial v(r)}\right) = \left(\frac{\partial \mu}{\partial v(r)}\right)_N = \left(\frac{\partial \rho(r)}{\partial N}\right)_{v(r)} \quad (1)$$

Here, $\rho(r)$ denoted the electron density at a spatial position r, N represented the total number of electrons in the system, and the partial derivative was evaluated under a constant external potential v. The condensed Fukui function, calculated on the distribution of electron density distribution around an atom, was here applied to simplify the calculations processes.[36] The condensed Fukui function can be obtained by eqn (2):

$$\text{Electrophilic attack: } f_k^- = q_N^k - q_{N-1}^k \quad (2)$$

where q_N^k represents the atom charge population of the atom k under a given electronic state, the f_k^- provide the information about different molecular locations. The larger the f_k^- value, the greater reaction activity of the site within the molecular.

2.5 Toxicity assay

The ecotoxicity of LMG and its products to aquatic organisms were predicted using both Ecological Structure–Activity Relationship (ECOSAR, version 2.2). ECOSAR program was developed by the US EPA, OECD and EU, which has been successfully used in the estimation of chemical toxicity including the LC50 to fish (96 h) and daphnia (48 h) and chronic toxicity values (Chv) for fish and daphnia.[37]

Additionally, the luminescent bacteria test was conducted to evaluate the acute toxicity of products during the degradation of LMG by heat/PDS treatment. Based on the previous work,[38] the bacteria PPT_3 was applied as the source of luminescence. The bacteria PPT_3 was activated by 2% NaCl solution, diluted by 3% NaCl solution, and then exposed to sample solutions for 15 min. Then Ensight Multimode Microplate Reader (PerkinElmer, MA, USA) was adopted to record the luminescence intensity, and the higher luminescence intensity represents the lower toxicity. Detailed procedures were displayed in Text S2.

3 Results and discussion

3.1 Degradation of LMG by heat/PDS oxidation

As illustrated in Fig. 1, no removal of LMG was observed in control experiments with heating or PDS alone over 180 min, revealing that direct PDS oxidation or volatilization did not contribute to LMG degradation. In contrast, LMG was effectively removed by heat/PDS oxidation (Fig. 1a). At the PDS concentration of 0.2 mM, approximately 44.2% of LMG was decomposed at 180 min. Increasing PDS concentration to 1 mM resulted in nearly complete removal over the same period, while further increasing to 0.2 mM shorten the time for complete degradation to 90 min. The degradation of LMG can be described by a pseudo-first-order kinetic model (Fig. S1), with the pseudo-first-order rate constant determined by the linear regression of $\ln([LMG]_0/[LMG]_t)$ against t at condition (eqn (3)):

$$\ln\frac{[LMG]_0}{[LMG]_t} = k_{obs}t \quad (3)$$

where $[LMG]_0$ and $[LMG]_t$ are the concentration of BPA at time 0 and t, respectively. In the condition of 1 mM PDS at 60 °C, the k_{obs} of LMG was calculated as 0.0255 min^{-1}. Increasing the PDS dosage to 2.0 mM raised k_{obs} to 0.0478 min^{-1}. This enhancement is attributed to greater generation of oxidizing species at higher PDS concentrations in heat/PDS treatment.

Temperature also played a vital role in LMG degradation in the heat/PDS oxidation (Fig. 1c and S2). Experiments conducted between 40 °C and 80 °C demonstrated a strong positive correlation between temperature and removal efficiency. The k_{obs} increased by a factor of 28.7 when the temperature was raised from 40 to 70 °C, consistent with previous findings on the degradation of atrazine in heat/PDS system.[31] When the temperature further increased to 80 °C, the increase in k_{obs} value became insignificant. This result suggested that practical application of heat/PDS for LMG contaminated water should balance efficiency with economic feasibility.

The temperature dependency of k_{obs} can be further evaluated by Arrhenius equation (eqn (4)):

$$\ln k_{obs} = -\frac{E_a}{RT} + \ln A \quad (4)$$

where E_a is apparent activation energy, R is the universal gas constant (8.314 J mol^{-1} K^{-1}), A is the pre-exponential factor, and T is the absolute temperature. Fig. 1d shows that $\ln k_{obs}$ is decreased linearly with increasing T^{-1}, revealing their relationship fitted well with Arrhenius equation.[39] Thus, the apparent activation energy (E_a) can be measured to be 88.7 kJ mol^{-1}, comparable to reported values, *i.e.* 108 kJ mol^{-1} for trichloroethene (TCE) and 64.8 kJ mol^{-1} for ciprofloxacin.[31] It is noteworthy that although higher temperature facilitated the degradation of LMG in heat/PDS oxidation, evaluated scavenging reactions and faster depletion of PDS may occur simultaneously, which may increase energy consumption. Thus, identifying an optimal temperature is crucial for successful remediation. Considering economic benefits and degradation efficiency simultaneously, 60 °C was selected as the reaction temperature for subsequent experiments in this work.

3.2 Reactive radical identification

Several research reported that various reactive species can be generated in heat/PDS system. $SO_4^{\bullet -}$ can be generated *via* activating PDS, which can react with H_2O or OH^- to generate $OH^{\bullet}$. Both $OH^{\bullet}$ and $SO_4^{\bullet -}$ could potentially attack LMG and lead

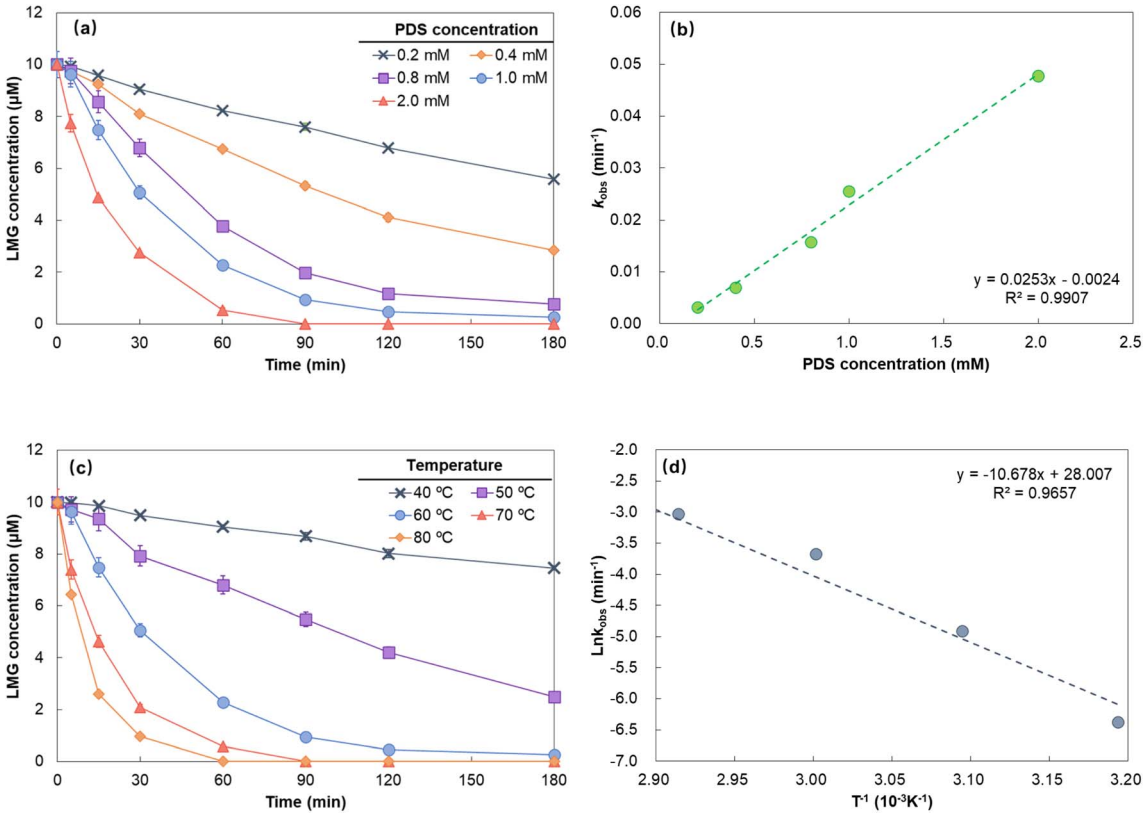

Fig. 1 Effect of PDS and temperature on the degradation of LMG by heat/PDS oxidation. Experimental conditions: LMG 10 μM, PDS 0.0–2.0 mM, pH 7.0, temperature 40–80 °C.

to degradation. In the condition of 1 mM PDS at 60 °C, nearly 100% LMG was decomposed with the k_{obs} of 0.0255 min^{-1}. To distinguish the roles of OH˙ and $SO_4^{\cdot-}$, MEOH and TBA were chosen as quenching agents. Generally, MEOH was known as a radical quencher for both OH˙ and $SO_4^{\cdot-}$ ($k_{MEOH,OH\cdot} = 9.7 \times 10^8$ M^{-1} s^{-1}, $k_{MEOH,SO_4^{\cdot-}} = 1.1 \times 10^7$ M^{-1} s^{-1}), while TBA was a selective quencher for OH˙ ($k_{TBA,OH\cdot} = 3.8 \times 10^8$ M^{-1} s^{-1}, $k_{TBA,SO_4^{\cdot-}} = 4 \times 10^5$ M^{-1} s^{-1}).[40] And the scavenging ratio of OH˙ and $SO_4^{\cdot-}$ by MEOH or TBA can be calculated as follows:

$$\text{Scavenging ratio(radical, \%)} = \frac{[\text{quencher}] \times k_{\text{quencher, radical}}}{[\text{gencher}] \times k_{\text{quencher, radical}} + [\text{LMG}] \times k_{\text{LMG, radical}}} \quad (5)$$

where [quencher] and [LMG] represent the concentrations of quencher (methanol or TBA) and LMG, respectively; $k_{quencher,radical}$ and $k_{LMG,radical}$ represent the second-order rate constant of radical reacting with quencher and LMG. The $k_{methanol,\cdot OH}$, $k_{TBA,\cdot OH}$ and $k_{LMG,\cdot OH}$ were 9.7×10^8 M^{-1} s^{-1}, 3.8×10^8 M^{-1} s^{-1} and 2.1×10^9 M^{-1} s^{-1}, respectively. The $k_{methanol,SO_4^{\cdot-}}$, $k_{TBA,SO_4^{\cdot-}}$ and $k_{LMG,SO_4^{\cdot-}}$ were 1.1×10^7 M^{-1} s^{-1}, 4.0×10^5 M^{-1} s^{-1} and 7.5×10^8 M^{-1} s^{-1}, respectively.[16,40] The Scavenging ratio of each radical was summarized in Table 1.

Consequently, introducing 10 mM MEOH into the reaction solution, 97.9% of OH˙ and 59.5% of $SO_4^{\cdot-}$ was scavenged (Table 1). Under this condition, 44.4% LMG was degraded at 180 min with the k_{obs} of 0.0034 min^{-1} (Fig. 2 and S3). Substitution MEOH with TBA resulted in about 94.8% of OH˙ and only 5.1% of $SO_4^{\cdot-}$

Table 1 Scavenging ratio of ˙OH or $SO_4^{\cdot-}$ in heat/PDS condition by MEOH or TBA

	Scavenging ratio	
	˙OH	$SO_4^{\cdot-}$
MEOH	97.9%	59.5%
TBA	94.8%	5.1%

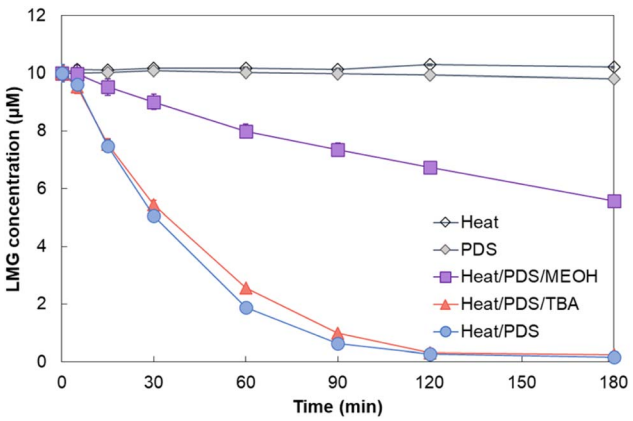

Fig. 2 Effect of MEOH or TBA on the degradation of LMG by heat/PDS oxidation. Experimental conditions: LMG 10 μM, PDS 1.0 mM, MEOH or TBA 10 mM, pH 7.0, temperature 60 °C.

being quenched, and the k_{obs} of LMG was 0.266 min^{-1} which extremely close to the k_{obs} obtained in heat/PDS system (Fig. 2 and S3). Above all, these results strongly signify the leading role of $SO_4^{\bullet-}$ in LMG degradation in heat/PDS system.

3.3 Effects of nontarget natural water constituents

3.3.1 Halides. Halides, especially Br^- and Cl^-, are ubiquitous in aquatic systems and may participate in radical mediated degradation in SR-AOPs.[41–44] Thus, their effects on LMG degradation were investigated over environmentally relevant concentrations.

As can be seen in Fig. 3a, the k_{obs} value of LMG decreased from 0.0255 min^{-1} to 0.0101 min^{-1} as Br^- concentration increased from 0.00 to 0.10 mM. This inhibition is due to the competition of Br^- with LMG for $SO_4^{\bullet-}$. It has been reported that Br^- can scavenge $SO_4^{\bullet-}$ to form $Br^\bullet$ at a secondary rate constant of 3.9×10^9 M^{-1} s^{-1},[45] then $Br^\bullet$ reacts with Br^- to form $Br_2^{\bullet-}$. Besides, the reaction of $Br^\bullet$ with H_2O/OH^- and Br^- with $HO^\bullet$ can generate $BrOH^{\bullet-}$ which further reacting with Br^- to form $Br^{\bullet-}$. Finally, $Br^{\bullet-}$ is readily transformed to free bromine. Both bromide radical and free bromine can be classified as reactive bromine species (RBS). Although it has been reported that RBS can serve as secondary oxidants, their oxidation potentials (1.6–2.2 V *vs.* NHE) are lower than that of $SO_4^{\bullet-}$, making them less effective in oxidizing LMG. Thus, the formation of RBS does not compensate for the loss of $SO_4^{\bullet-}$, leading to net inhibition.

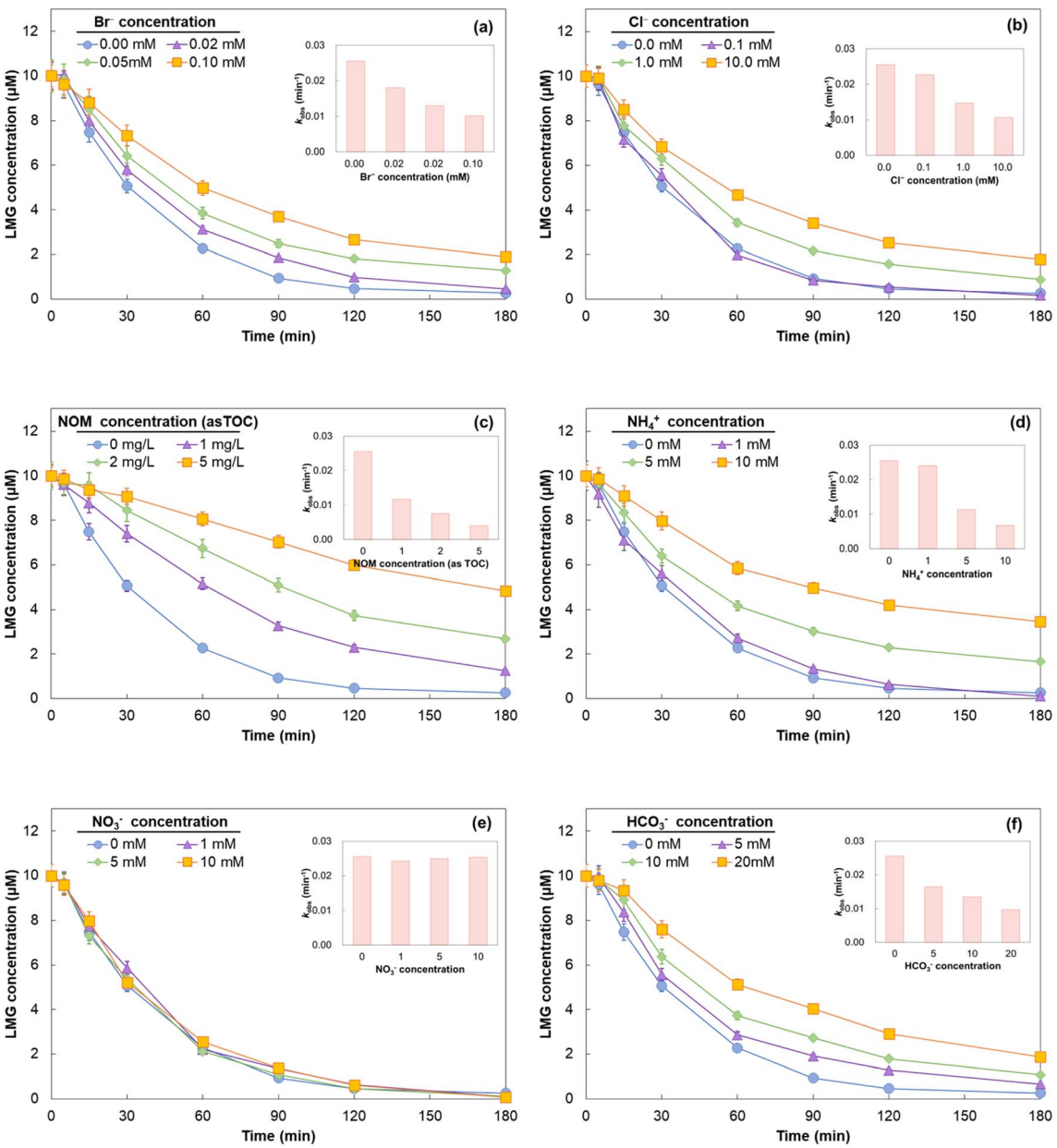

Fig. 3 Effect of (a) Br^-, (b) Cl^-, (c) NOM, (d) NH_4^+, (e) NO_3^- and (f) HCO_3^- on the degradation of LMG by heat/PDS oxidation. Experimental conditions: LMG 10 μM, PDS 1.0 mM, Br^- 0.0–0.1 mM, Cl^- 0–10.0 mM, NOM 0–5 mg L^{-1} (as TOC), NH_4^+ 0–10 mM, NO_3^- 0–10 mM, HCO_3^- 0–20 mM, pH 7.0, temperature 60 °C.

The effect of Cl^- on LMG degradation was also explored. The k_{obs} value was 0.0226 min^{-1} in the presence of 0.1 mM Cl^-, similiar to the control experiment (Fig. 3b). The bimolecular rate constant of Cl^- reacting with $SO_4^{\bullet-}$ is 2.7×10^8 M^{-1} s^{-1},[45] close to that of LMG (7.5×10^8 M^{-1} s^{-1}), indicating limited competition at low Cl^- level. However, in the presence of higher concentration of Cl^- (10 mM), the k_{obs} value dropped to 0.0106 min^{-1}, suggesting the effective quenching of $SO_4^{\bullet-}$ at higher Cl^- concentration

$$X^- + SO_4^{\bullet-} \rightleftharpoons X^\bullet + SO_4^{2-} \quad (R1)$$

$$X^\bullet + X^- \rightleftharpoons X_2^{\bullet-} \quad (R2)$$

$$X_2^{\bullet-} + Br^\bullet \rightleftharpoons X_2 + X^- \quad (R3)$$

$$X^\bullet + X^\bullet \rightleftharpoons X_2 \quad (R4)$$

$$X_2 + H_2O \rightleftharpoons HXO + H^+ + X^- \quad (X = Cl^- \text{ or } Br^-) \quad (R5)$$

3.3.2 NOM. NOM, a mixture of macromolecular organic compounds prevalent in natural environments, widely distributed in surface waters and groundwaters.[46] Suwannee River NOM was adopted to assess the role of NOM on LMG degradation in heat/PDS treatment. As can be seen in Fig. 3c, the addition of NOM can obviously hinder the degradation of LMG. After 180 min reaction, the degradation efficiency and k_{obs} values decreased from 97.37% and 0.0255 min^{-1} in the blank experiment to 73.14% and 0.0075 min^{-1}, respectively, at a NOM concentration of 2 mg L^{-1} (as TOC) (Fig. 3c). NOM macromolecules comprise a variety of covalently bonded aromatic and aliphatic moieties,[47] which are susceptible to be attacked by $SO_4^{\bullet-}$ to generate small-molecular organic fractions, which may compete with the parent pollutants. Hou *et al.* reported that SRNOM could react with $SO_4^{\bullet-}$ at a secondary order rate constant of $(1.53 \pm 0.058) \times 10^3$ L per mgC per s, consequently reducing availability of $SO_4^{\bullet-}$ for LMG.[48] Overall, the inhibitory effect of NOM on the degradation of LMG was primarily ascribed to its scavenging action of $SO_4^{\bullet-}$.

3.3.3 Nitrogenous ions. NH_4^+ and NO_3^- are common nitrogenous ions, widespread in various water environments, their concentrations usually reaching several milligrams per liter in groundwater and even higher in eutrophicated waters.[49] Fig. 3d showed that the addition of NH_4^+ retarded the LMG degradation, and the retarding effect became more significant with the increased NH_4^+ concentration. In the presence of 10 mM NH_4^+, the k_{obs} value was only 0.0067 min^{-1}. This phenomenon was the result of the competition of NH_4^+ with LMG for $SO_4^{\bullet-}$.[50,51] As reported, NH_4^+ can react with $SO_4^{\bullet-}$ to form aminyl radical ($NH_2^\bullet$) at a bimolecular reaction rate constant of 3.5×10^5 M^{-1} s^{-1}.[45] Although the value is three orders of magnitude lower than that of LMG reacting with $SO_4^{\bullet-}$ (7.5×10^8 M^{-1} s^{-1}), the NH_4^+ concentration (mM level) in the solution was hundreds of times higher than LMG concentration (10 μM). This enabled NH_4^+ to compete for $SO_4^{\bullet-}$ and thus suppressed the degradation of LMG. As to NO_3^-, its bimolecular reaction rate constant with $SO_4^{\bullet-}$ was only 2.1 M^{-1} s^{-1},[45] implying that NO_3^- hardly participated in the reaction. As can be seen in Fig. 3e, the effect of NO_3^- on LMG degradation in heat/PDS oxidation process can be neglected.

$$NH_4^+ + SO_4^{\bullet-} \rightleftharpoons NH_2^\bullet + SO_4^{2-} + 2H^+ \quad (R6)$$

3.3.4 HCO_3^-. The effect of different concentrations of HCO_3^- on heat/PDS oxidation of LMG was investigated and the results are shown in Fig. 3f. The degradation efficiency of LMG in the presence of 10 mM HCO_3^- after 180 min reaction is 89.20%, slightly lower than that in the absence of HCO_3^-. The k_{obs} decreased from 0.0255 min^{-1} to 0.0097 min^{-1}, as HCO_3^- concentration increased from 0 to 20 mM. Such results may be attributed to reaction between HCO_3^- and $SO_4^{\bullet-}$ to generate weaker carbonate radical ($CO_3^{\bullet-}$). Compared with $SO_4^{\bullet-}$, $CO_3^{\bullet-}$ has a lower redox potential (1.59–1.78 V *vs.* SHE), thus cannot make for LMG degradation in heat/PDS oxidation.[29]

$$HCO_3^- + SO_4^{\bullet-} \rightleftharpoons CO_3^\bullet + SO_4^{2-} + H^+ \quad (R7)$$

3.4 Mineralization and products transformation

Synchronous mineralization was also adopted to indicate the performance of heat/PDS treatment. In presence of 2 mM PDS, complete removal of LMG required approximately 90 min, while the TOC removal stood at 20.59%. Extending the reaction time to 180 min enhanced the mineralization ratio to 51.76%. The mineralization extent reached 75.29% after 360 min reaction (Fig. S5). Overall, the LMG can be effectively mineralized by appropriately increasing reaction time, highlighting the adaptive conditions for the application of SR-AOPs.

Degradation products and transformation pathways were investigated *via* theoretical calculation and MS analysis, (Table S1). Based on the radical quenching experiments above, $SO_4^{\bullet-}$ was confirmed as the dominate oxidant for LMG degradation. It is well known that $SO_4^{\bullet-}$, as an electrophilic oxidant, preferentially attacks electron-rich sites *via* single-electron transfer. The highest occupied molecular orbital (HOMO) distribution shows the electron-rich sites of the molecular structure.[52] In another word, HOMO indicates easy escape of electron which can be easily attacked by $SO_4^{\bullet-}$. As can be seen Fig. 4b, the HOMO mainly localized on the triazine ring and amino functional groups, revealing these sites highly prone to electrophilic attacks. This electron distribution results from the activation of triazine ring through electron-donating amino substituents, while benzene ring is deactivated by electron-withdrawing chlorine atoms.

To further evaluate the vulnerable sites of LMG, the Fukui index (f^{-1}) was employed. A higher f^{-1} value means a higher reactivity.[53,54] Fig. 4c shows the N16 atom of the amino group is the most reactive site on LMG with f^{-1} of 0.665, suggesting it is the most vulnerable for $SO_4^{\bullet-}$ attack, followed by electron migration to C12, oxygen addition, and superoxide elimination to yield an imine intermediate (Fig. S4). Subsequent hydrolysis produces deaminated and hydroxylated products (Fig. 5, Pathway2, P3[a]). Fig. 4c shows that the f^{-1} value of another two sites, N13 and N15, ranked only second to N16 (0.569 and 0.542, respectively), suggesting these sites are also susceptible to $SO_4^{\bullet-}$ oxidation. For N15, two degradation pathways might occur. One

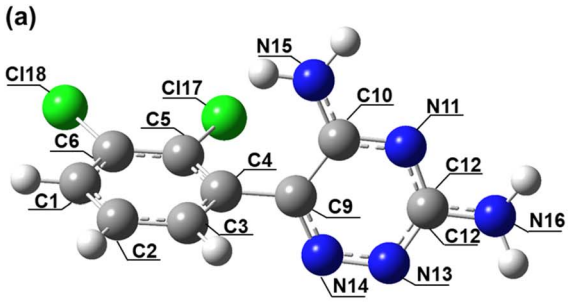

(c)

Atom	Site	f^-
C	1	0.139
C	2	0.118
C	3	0.124
C	4	0.020
C	5	0.049
C	6	0.041
Cl	7	-0.008
Cl	8	-0.006
C	9	0.263
C	10	-0.236
N	11	0.293
C	12	-0.316
N	13	0.569
N	14	0.044
N	15	0.542
N	16	0.665
H	17	-0.142
H	18	-0.137
H	19	-0.136
H	20	-0.225
H	21	-0.227
H	22	-0.217
H	23	-0.219

Fig. 4 (a) Molecular structure, (b) HOMO and (c) electrophilic Fukui index of LMG.

possibility is that the single-electron oxidation on N15 formed an N15-centered radical which underwent oxidation and hydrolysis giving rise to another de-amino and hydroxylated products (Fig. 5, Pathway2, P3[b]). Alternatively, the electron on N15-centered radical might undergo intramolecular transfer to the dichlorophenyl ring, facilitating the addition of N15 to C3 and leading to the formation of a tricyclic heteroaromatic product (Fig. 5c, Pathway1, P1). Similar cyclization products have been reported during the photodegradation of LMG, and such addition reactions *via* single-electron oxidation are known

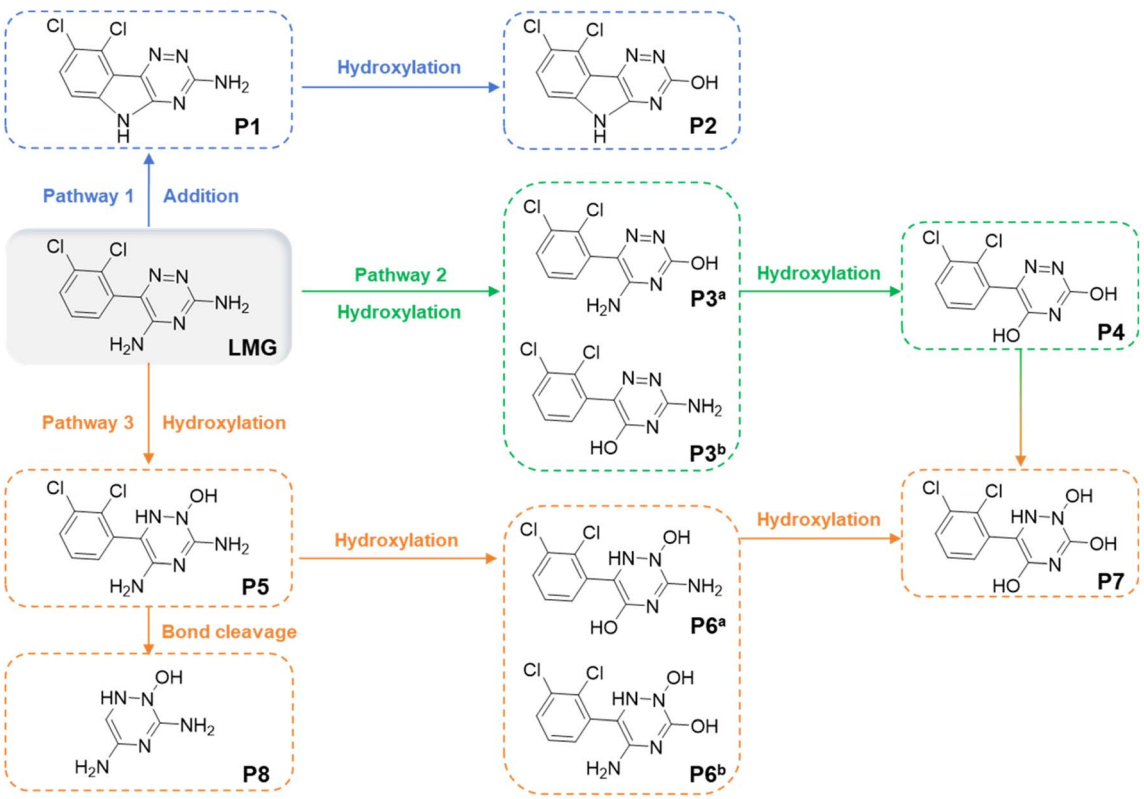

Fig. 5 Degradation pathway of LMG in heat/PDS system.

Table 2 Toxicity evaluation of LMG and its degradation products by ECOSAR

	Acute toxicity			Chronic toxicity		
	Fish	Daphnid	Green algae	Fish	Daphnid	Green algae
LMG	3.64	0.53	0.294	0.115	0.053	0.113
P1	4.3	2.91	4.43	0.516	0.459	1.71
P2	55	20.9	68.7	5.29	2.17	9.49
P3[a]	13	1.08	2.14	0.122	0.225	0.362
P3[b]	5.52	0.734	1.07	0.062	0.145	0.195
P4	6.9	44.2	3.65	3.52	16	0.526
P5	21 700	10 100	3220	1670	556	535
P6[a]	872	466	271	79.4	38.4	61.9
P6[b]	2 910 000	1 080 000	141 000	173 000	32 600	14 400
P7	2 890 000	1 080 000	140 000	172 000	32 400	14 300
P8	1 270 000	473 000	62 200	75 500	14 400	6400

to occur on aromatic systems.[18] In Pathway3, degradation was initiated on N13 by $SO_4^{\bullet-}$ attack, leading to the formation of P5.

P1, P3[a], P3[b] and P5 were identified as primary products. P3[a] and P3[b] are geometric isomers, due to the lack of authentic standards, their formation cannot be distinguished and quantified. Thus, the sum of the abundance of these two MS peaks can be applied to exhibit their generation trends. As can be seen in Fig. S6, the sum of P3[a] and P3[b] increased to a temporal maximum at 60 min, then gradually decreased. Such results implied that they were the crucial intermediates and can be further oxidized by $SO_4^{\bullet-}$. P3 (both P3[a] and P3[b]) and P4 shared the same core scaffold, differing only by the replacement of an amino group in P3 with a hydroxyl group in P4, suggesting that P3 undergoes deamination and hydroxylation to yield P4. Likewise, P1 and P5 exhibited similar formation trends (Fig. 5). Hydroxylation of P1 and P5 gave rise to P2 and P6 (both P6[a] and P6[b]), respectively. P4 and P6 underwent further oxidation contributed to P7. Additionally, P5 may undergo C–C bond cleavage to release 2-hydroxy-3,5-diamino triazine (P8).

3.5 Toxicity evaluation

The ecological safety of heat/PDS treatment was assessed by predicting the acute and chronic toxicity of LMG and its degradation products using the ECOSAR software. All the organic compounds were given in the unit of mg L^{-1}, which can be classified as four toxicity grades, *e.g.*, not harmful (>100.0), harmful (10.0–100.0), toxic (1.0–10.0), and very toxic (<1.0). Table 2 displays the predict acute and chronic toxicity to fish, daphnid, and green algae. The acute LC_{50} values of the parent LMG to Daphnid and green algae were 0.53 and 0.294 mg L^{-1}, respectively, implying its high toxicity. The chronic toxicity of LMG to fish, daphnid, and green algae was in a very toxic degrade as well. Although P1 and P3 showed lower toxicity than LMG, their predicted acute and chronic toxicity remained between the very toxic and harmful categories (Table 2). In contrast, the polyhydroxylated products (P5–P8) displayed substantially reduced toxicity to fish, daphnid, and green algae, with most values reaching the not harmful grade. This trend indicates that progressive hydroxylation during LMG degradation generates less toxic compounds, and extended reaction times favor the further oxidation of primary intermediates.

Furthermore, the toxicity during LMG degradation process *via* heat/PDS treatment was evaluated by luminescence bacterium test, where lower luminescence intensity corresponds to higher toxicity. Initially, LMG was the sole compound in the reaction

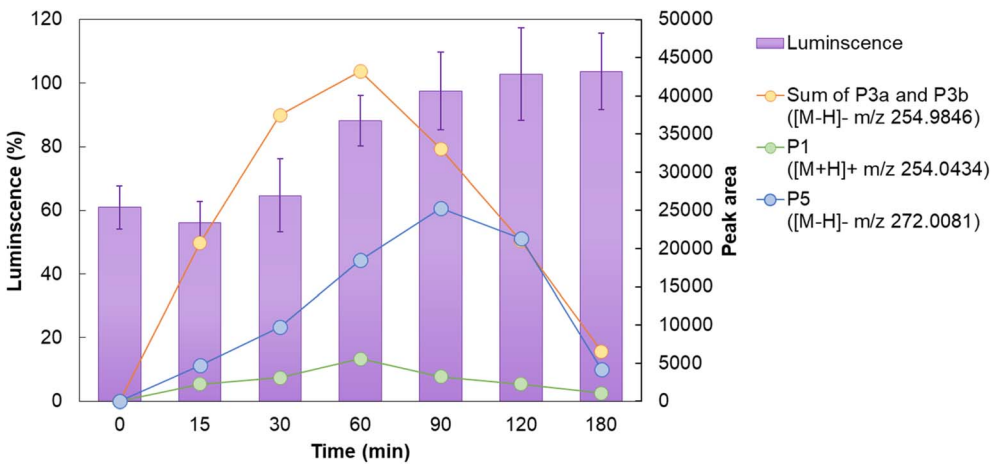

Fig. 6 The luminescence intensity of PPT_3 in LMG sample following heat/PDS oxidation. Experimental conditions: LMG 10 μM, PDS 1.0 mM, pH 7.0, temperature 60 °C.

solution, and the luminescence intensity of bacteria PPT_3 was 60.98%, indicating its moderate acute toxicity. After 60 min reaction, the luminescence intensity slightly increased to 64.75%, with the toxic intermediates (P1 and P3) reaching their maximum abundances (Fig. 6). Based on ECOSAR prediction, their predicted toxicity remains relatively high, which explains the limited change in luminescence at this time point. As the reaction proceeded to 180 min, the luminescence intensity rose to 103.69%, signifying the disappearance of acute toxicity. This detoxification coincided with the substantial decline of primary products, and the subsequent products (*i.e.* P6–P8) classified as not harmful *via* ECOSAR software. The temporal correlation between the depletion of toxic intermediates strongly suggests that the detoxification is driven by the transformation of LMG and primary products into polyhydroxylated derivatives.

Overall, the experimental data align well with ECOSAR predictions and demonstrated that prolonged treatment effectively converts toxic intermediates into innocuous products. It should be noted that toxicological performance can be affected by multiple combined factors and small changes in treatment. Additionally, the particularities of degradation products physicochemical characteristics and living organisms environmental interaction also led to different toxicological responses. Thus, it is suggested that further tests should be conducted to ensure the ecological safety of effluent disposal.

4 Conclusion

This study found that LMG can be effectively degraded by heat/PDS treatment. The degradation process follows pseudo-first-order kinetics, with the rate constants increasing with higher PDS dosage and temperature. $SO_4^{\bullet-}$ were identified as the dominant reactive species responsible for the LMG oxidation. The co-existing halides, NOM, NH_4^+ or HCO_3^- served as scavengers of $SO_4^{\bullet-}$ and suppressed the degradation, while NO_3^- exert an insignificant influence on LMG degradation. Dependent on the DFT calculations and HRMS analysis, three possible degradation pathways were proposed, including addition, hydroxylation and ring cleavage. Both ECOSAR results and luminescence bacterium test showed that most of products are less toxic than the parent LMG, thus heat/PDS treatment can be used as an effective technique to detoxify the LMG-contaminated water.

Author contributions

Jiayue Dong: investigation, formal analysis, data curation, writing – original draft, conceptualization, funding acquisition. Jing Wu: writing – review & editing. Jialing Zhang: writing – review & editing. Zhuoming Deng: formal analysis, data curation. Guoqiang Liu: writing – review &editing, funding acquisition. Yonghua Liu: writing – review &editing, funding acquisition.

Conflicts of interest

The authors declare that they have no known competing financial interests or personal relationships that could have appeared to influence the work reported in this paper.

Data availability

The data that support the findings of this study are available on reasonable request from the corresponding author.

Supplementary information (SI): SPE procedures, luminescent bacteria test procedures, and MS data of samples. See DOI: https://doi.org/10.1039/d5ra09514j.

Acknowledgements

This research was supported by the Special Fund of Chinese Central Government for Basic Scientific Research Operations in Commonweal (GYZX250207). The contents of the paper do not necessarily represent the views of the funding agency.

References

1 A. F. Cohen, G. S. Land, D. D. Breimer, W. C. Yuen, C. Winton and A. W. Peck, Lamotrigine, a new anticonvulsant: Pharmacokinetics in normal humans, *Clin. Pharmacol. Ther.*, 1987, **42**, 535–541.
2 B. Zonja, A. Delgado, J. L. Abad, S. Pérez and D. Barceló, Abiotic amidine and guanidine hydrolysis of lamotrigine-N2-glucuronide and related compounds in wastewater: The role of pH and N2-substitution on reaction kinetics, *Water Res.*, 2016, **100**, 466–475.
3 B. Zonja, S. Pérez and D. Barceló, Human Metabolite Lamotrigine-N2-glucuronide Is the Principal Source of Lamotrigine-Derived Compounds in Wastewater Treatment Plants and Surface Water, *Environ. Sci. Technol.*, 2015, **50**, 154–164.
4 I. Ferrer and E. M. Thurman, Identification of a New Antidepressant and its Glucuronide Metabolite in Water Samples Using Liquid Chromatography/Quadrupole Time-of-Flight Mass Spectrometry, *Anal. Chem.*, 2010, **82**, 8161–8168.
5 I. Ferrer and E. M. Thurman, Analysis of 100 pharmaceuticals and their degradates in water samples by liquid chromatography/quadrupole time-of-flight mass spectrometry, *J. Chromatogr. A*, 2012, **1259**, 148–157.
6 T. Filep, L. Szabó, A. C. Kondor, G. Jakab and Z. Szalai, Evaluation of the effect of the intrinsic chemical properties of pharmaceutically active compounds (PhACs) on sorption behaviour in soils and goethite, *Ecotoxicol. Environ. Saf.*, 2021, **215**, 112120.
7 D. Montenegro-Apraez, C. A. L. Graça, F. Machuca-Martinez and O. S. G. P. Soares, Catalytic ozonation of lamotrigine with modified activated carbon: degradation, mineralization and by-products analysis, *J. Water Process Eng.*, 2025, **77**, 108434.
8 <LMG concentration 3 + toxicity on human being.pdf>.
9 V. Baldasso, S. Sayen, C. A. R. Gomes, L. Frunzo, C. M. R. Almeida and E. Guillon, Metformin and lamotrigine sorption on a digestate amended soil in presence of trace metal contamination, *J. Hazard. Mater.*, 2024, **466**, 133635.

10 T. Malchi, Y. Maor, G. Tadmor, M. Shenker and B. Chefetz, Irrigation of Root Vegetables with Treated Wastewater: Evaluating Uptake of Pharmaceuticals and the Associated Human Health Risks, *Environ. Sci. Technol.*, 2014, **48**, 9325–9333.

11 A. Paz, G. Tadmor, T. Malchi, J. Blotevogel, T. Borch, T. Polubesova and B. Chefetz, Fate of carbamazepine, its metabolites, and lamotrigine in soils irrigated with reclaimed wastewater: Sorption, leaching and plant uptake, *Chemosphere*, 2016, **160**, 22–29.

12 Y. Bigott, S. P. Chowdhury, S. Pérez, N. Montemurro, R. Manasfi and P. Schröder, Effect of the pharmaceuticals diclofenac and lamotrigine on stress responses and stress gene expression in lettuce (Lactuca sativa) at environmentally relevant concentrations, *J. Hazard. Mater.*, 2021, **403**, 123881.

13 H. Yang, X. Gu, H. Chen, Q. Zeng, Z. Mao and Y. Ge, Omics techniques reveal the toxicity mechanisms of three antiepileptic drugs to juvenile zebrafish (Danio rerio) brain and liver, *Aquat. Toxicol.*, 2023, **262**, 106668.

14 A. F. Bollmann, W. Seitz, C. Prasse, T. Lucke, W. Schulz and T. Ternes, Occurrence and fate of amisulpride, sulpiride, and lamotrigine in municipal wastewater treatment plants with biological treatment and ozonation, *J. Hazard. Mater.*, 2016, **320**, 204–215.

15 M. Engel and B. Chefetz, Removal of triazine-based pollutants from water by carbon nanotubes: Impact of dissolved organic matter (DOM) and solution chemistry, *Water Res.*, 2016, **106**, 146–154.

16 O. S. Keen, I. Ferrer, E. Michael Thurman and K. G. Linden, Degradation pathways of lamotrigine under advanced treatment by direct UV photolysis, hydroxyl radicals, and ozone, *Chemosphere*, 2014, **117**, 316–323.

17 N. Klanovicz, J. M. S. de Jesus, F. M. Costa, G. C. de Assis, B. Ramos, A. F. Camargo, W. Michelon, A. Dallegrave, R. W. Becker, H. Treichel and A. C. S. C. Teixeira, A novel hybrid continuous-flow wastewater treatment for lamotrigine degradation by combining enzymatic and photo-oxidative reactions, *J. Water Process Eng.*, 2023, **56**, 104395.

18 R. B. Young, B. Chefetz, A. Liu, Y. Desyaterik and T. Borch, Direct photodegradation of lamotrigine (an antiepileptic) in simulated sunlight – pH influenced rates and products, *Environ. Sci.: Processes Impacts*, 2014, **16**, 848–857.

19 M. Karpov, B. Seiwert, V. Mordehay, T. Reemtsma, T. Polubesova and B. Chefetz, Abiotic Transformation of Lamotrigine by Redox-Active Mineral and Phenolic Compounds, *Environ. Sci. Technol.*, 2021, **55**, 1535–1544.

20 L. Liu, H. Yan, C. Yang and G. Zhu, Dewatering of drilling sludge by ultrasound assisted Fe(ii)-activated persulfate oxidation, *RSC Adv.*, 2018, **8**, 29756–29766.

21 P. V. Nidheesh, G. Divyapriya, F. Ezzahra Titchou and M. Hamdani, Treatment of textile wastewater by sulfate radical based advanced oxidation processes, *Sep. Purif. Technol.*, 2022, **293**, 121115.

22 Z. Zhang, X. Yue, Y. Duan and Z. Rao, A study on the mechanism of oxidized quinoline removal from acid solutions based on persulfate–iron systems, *RSC Adv.*, 2020, **10**, 12504–12510.

23 X. Zhou, Z. Guo, X. Tang, W. Wang, M. Wu, B. Song, Y. Xiang, Y. Li, W. Xiong, D. Huang and C. Zhou, Sulfate radical-based advanced oxidation processes for simultaneous removal of antibiotic-resistant bacteria and antibiotic resistance genes and the affecting factors, *Chem. Eng. J.*, 2024, **498**, 155149.

24 Y. Gao, Y. Zhu, T. Li, Z. Chen, Q. Jiang, Z. Zhao, X. Liang and C. Hu, Unraveling the High-Activity Origin of Single-Atom Iron Catalysts for Organic Pollutant Oxidation via Peroxymonosulfate Activation, *Environ. Sci. Technol.*, 2021, **55**, 8318–8328.

25 T. Zeng, X. Tang, Z. Huang, H. Chen, S. Jin, F. Dong, J. He, S. Song and H. Zhang, Atomically Dispersed Fe–N4 Site as a Conductive Bridge Enables Efficient and Stable Activation of Peroxymonosulfate: Active Site Renewal, Anti-Oxidative Capacity, and Pathway Alternation Mechanism, *Environ. Sci. Technol.*, 2023, **57**, 20929–20940.

26 R. Zhang, P. Sun, T. H. Boyer, L. Zhao and C.-H. Huang, Degradation of Pharmaceuticals and Metabolite in Synthetic Human Urine by UV, UV/H-$_2O_2$, and UV/PDS, *Environ. Sci. Technol.*, 2015, **49**, 3056–3066.

27 S. Padmaja, Z. B. Alfassi, P. Neta and R. E. Huie, Rate constants for reactions of $SO_4^{\bullet-}$ radicals in acetonitrile, *Int. J. Chem. Kinet.*, 2004, **25**, 193–198.

28 U. Ushani, X. Lu, J. Wang, Z. Zhang, J. Dai, Y. Tan, S. Wang, W. Li, C. Niu, T. Cai, N. Wang and G. Zhen, Sulfate radicals-based advanced oxidation technology in various environmental remediation: A state-of-the–art review, *Chem. Eng. J.*, 2020, **402**, 126232.

29 C. Wang, J. Yan, J. Yuan, L. Zhang, W. Qian, G. Bian, Y. Song, X. Gao and H. Mao, Degradation of bisphenol A during heat-activated peroxodisulfate treatment: kinetics, mechanism, and transformation products, *RSC Adv.*, 2025, **15**, 28949–28958.

30 X. Chen, C. Hu, F. Hong, Y. Fang, X. Yuan, H. Tian and Y. Huang, Activation of persulfate with hydrodynamic cavitation in the removal of atrazine: Regulating the concentration of $^{\bullet}OH$ and $SO_4^{\bullet-}$ and the degradation mechanism, *J. Water Process Eng.*, 2024, **65**, 105828.

31 Y. Ji, Y. Shi, W. Dong, X. Wen, M. Jiang and J. Lu, Thermo-activated persulfate oxidation system for tetracycline antibiotics degradation in aqueous solution, *Chem. Eng. J.*, 2016, **298**, 225–233.

32 B. Liu, Y. Wang, X. Hao, X. Liang and Q. Yang, Activation of PMS degradation of chlorotriazine herbicides (atrazine and simazine) by MIL101-derived Fe/Co@C under high salinity conditions, *Chem. Eng. J.*, 2023, **475**, 146129.

33 W. Ren, X. Huang, L. Wang, X. Liu, Z. Zhou, Y. Wang, C. Lin, M. He and W. Ouyang, Degradation of simazine by heat-activated peroxydisulfate process: A coherent study on kinetics, radicals and models, *Chem. Eng. J.*, 2021, **426**, 131876.

34 W. Langenaeker, K. Demel and P. Geerlings, Quantum-chemical study of the Fukui function as a reactivity index: Part 3. Nucleophilic addition to α,β-unsaturated compounds, *J. Mol. Struct.: THEOCHEM*, 1992, **259**, 317–330.

35 K. Fukui, T. Yonezawa and H. Shingu, A molecular orbital theory of reactivity in aromatic hydrocarbons, *J. Chem. Phys.*, 1952, **20**, 722–725.
36 A. M. Elhorri, K. D. Belaid, M. Zouaoui-Rabah and R. Chadli, Theoretical study of the azo dyes dissociation by advanced oxidation using Fukui indices. DFT calculations, *Comput. Theor. Chem.*, 2018, **1130**, 98–106.
37 C. Chen, Y. Lu, J. Liang, L. Wang and J. Fang, Roles of nitrogen dioxide radical ($^{\bullet}NO_2$) in the transformation of aniline by sulfate radical and hydroxyl radical systems with the presence of nitrite, *Chem. Eng. J.*, 2023, **451**, 138755.
38 J. Dong, P. Yang, D. Kong, Y. Song and J. Lu, Formation of nitrated naphthalene in the sulfate radical oxidation process in the presence of nitrite, *Water Res.*, 2024, **255**, 121546.
39 A. Tsitonaki, B. Petri, M. Crimi, H. MosbÆK, R. L. Siegrist and P. L. Bjerg, In Situ Chemical Oxidation of Contaminated Soil and Groundwater Using Persulfate: A Review, *Crit. Rev. Environ. Sci. Technol.*, 2010, **40**, 55–91.
40 L. Gao, Y. Guo, J. Zhan, G. Yu and Y. Wang, Assessment of the validity of the quenching method for evaluating the role of reactive species in pollutant abatement during the persulfate-based process, *Water Res.*, 2022, **221**, 118730.
41 Y. Huang, J. Ren, Y. Wang, J. Fu, Y. Hou, B. Yang, L. Lei, A. Al-Anazi, G. Jiang and Z. Li, New insights into activation mechanisms of peroxymonosulfate by halide ions for micropollutant abatement: The generation routes and contributions of reactive radicals and hypohalous acid, *Chem. Eng. Sci.*, 2025, **305**, 121178.
42 K. Liu, J. Lu and Y. Ji, Formation of brominated disinfection by-products and bromate in cobalt catalyzed peroxymonosulfate oxidation of phenol, *Water Res.*, 2015, **84**, 1–7.
43 J. Lu, J. Wu, Y. Ji and D. Kong, Transformation of bromide in thermo activated persulfate oxidation processes, *Water Res.*, 2015, **78**, 1–8.
44 H. V. Lutze, N. Kerlin and T. C. Schmidt, Sulfate radical-based water treatment in presence of chloride: formation of chlorate, inter-conversion of sulfate radicals into hydroxyl radicals and influence of bicarbonate, *Water Res.*, 2015, **72**, 349–360.
45 P. Neta, R. E. Huie and A. B. Ross, Rate constants for reactions of inorganic radicals in aqueous solution, *J. Phys. Chem. Ref. Data*, 1988, **17**, 1027–1284.
46 X. Lei, Y. Lei, J. Guan, P. Westerhoff and X. Yang, Kinetics and transformations of diverse dissolved organic matter fractions with sulfate radicals, *Environ. Sci. Technol.*, 2022, **56**, 4457–4466.
47 M. Sillanpää, A. Matilainen and T. Lahtinen, in *Natural Organic Matter in Water*, 2015, pp. 17–53, DOI: 10.1016/b978-0-12-801503-2.00002-1.
48 S. Hou, L. Ling, D. D. Dionysiou, Y. Wang, J. Huang, K. Guo, X. Li and J. Fang, Chlorate formation mechanism in the presence of sulfate radical, chloride, bromide and natural organic matter, *Environ. Sci. Technol.*, 2018, **52**, 6317–6325.
49 J. Xin, Y. Liu, F. Chen, Y. Duan, G. Wei, X. Zheng and M. Li, The missing nitrogen pieces: A critical review on the distribution, transformation, and budget of nitrogen in the vadose zone-groundwater system, *Water Res.*, 2019, **165**, 114977.
50 P. Yang, Y. Ji and J. Lu, Transformation of ammonium to nitrophenolic byproducts by sulfate radical oxidation, *Water Res.*, 2021, **202**, 117432.
51 J. Liu, P. Yang, Y. Ji and J. Lu, Ammonium changes the pathway of tetrabromobisphenol S degradation by sulfate radical oxidation, *Chem. Eng. J.*, 2023, **475**, 146116.
52 L. Meng, J. Dong, J. Chen, L. Li, Q. Huang and J. Lu, Activation of peracetic acid by spinel $FeCo_2O_4$ nanoparticles for the degradation of sulfamethoxazole, *Chem. Eng. J.*, 2023, **456**, 141084.
53 Y. Feng, J. Ren, H. Li, D. Zhao, L. Sheng, Y. Wu, W. Zhao and M. Deng, Effect of thermal annealing on gas separation performance and aggregation structures of block polyimide membranes, *Polymer*, 2021, **219**, 123538.
54 R. Pino-Rios, O. Yanez, D. Inostroza, L. Ruiz, C. Cardenas, P. Fuentealba and W. Tiznado, Proposal of a simple and effective local reactivity descriptor through a topological analysis of an orbital-weighted fukui function, *J. Comput. Chem.*, 2017, **38**, 481–488.